Design and Modeling of Fabric-Shelled Pneumatic Bending Soft Actuators

Diego Quevedo-Moreno and Ellen T. Roche

***Abstract*—In recent years, the use of fabric to manufacture and integrate soft actuators and sensors into wearable robots elucidates the benefits of soft robotic technology, closing the gap between humans and machines. However, many limitations in terms of ease of manufacturing, customization, modeling, output force and control remain unsolved and reduce the number of practical applications of fabric-based soft robotic systems. To address these limitations, we propose the use of laser-cut fabric shells laminated onto thermoplastic polyurethane as a pneumatic bending soft actuator. In this letter the design, fabrication, modeling, and control of a fabric shelled bending actuator is presented. Our experiments suggest that the fabric-shelled actuators are highly tunable and usable for high force applications. Moreover, the finite element model developed can predict the behavior of different fabric shelled actuator designs. Finally, we show how precise control of the actuators can be achieved by the implementation of a feedback curvature control system.**

***Index Terms*—Soft robot materials and design, soft sensors and actuators, modeling, control, and learning for soft robots.**

I. Introduction

SOFT robotic systems have shown many advantages over conventional rigid robotic systems, such as low-cost, lightweight, high compliance and versatile locomotion and manipulation [1]. These characteristics enable safe interaction with unknown environments, often useful in human-centered tasks [2]. In recent years, the use of fabric to manufacture and integrate soft actuators and sensors into wearable robots elucidates the benefits of soft robotic technology, closing the gap between humans and machines [3]. However, many limitations remain unsolved and reduce the applications of fabric-based soft robotic systems: 1) the design and modeling of these fabric-based actuators is commonly an iterative process due to the complexity of predicting the non-intuitive behavior of soft materials [4], [5]; 2) the output force/torque is low for practical applications (around 10–15 N) [6]; 3) their fabrication is generally complicated and requires custom machines and expertise to manipulate them [7]; and 4) the precise control of soft actuators is challenging due to its continuous and soft nature [4]. Here, the design, manufacture, modeling, and control of a customizable fabric-shelled pneumatic bending soft actuator that addresses some of these limitations is presented.

Previously described fabric-based pneumatic bending actuators have shown their ability to twist, elongate/contract and bend [7]. Wearable robots often require complex motions, like bending [3]. Multiple strategies to achieve bending motion have been developed: attaching arrays of woven pouches to an inextensible layer [8], stitching and bonding of woven fabric for unfolding multi-chamber actuators [5], pleating and gathering of a single piece of fabric to direct unfold when inflated [9], [10], and combining knitted fabric with woven fabric [11]. The latter technique has demonstrated ability to reduce the number of actuators and complexity of fabrication in wearable robots, compared to other techniques [3]. Bending actuators utilize a knit anisotropic stretchable fabric, that allows preferential deformation in one direction, and a woven fabric, that acts as a strain-limiting layer to restrict linear extension [11]. Under pressurization, the knitted fabric is stretched and the strain-limiting layer constrains the expansion and transforms it into bending motion [6]. Variations on the design include using woven fabric reinforcements on knitted fabric to program the motion [12], [13]. However, none of the reported knitted fabric-based designs [7], [10], [11], [12], [13], [14] present how the variation of the geometrical parameters affects the bending motion of the actuator, which is crucial to understand to generate more deterministic designs in the future.

Moreover, modeling this type of actuator is challenging due to the inherent anisotropy induced by the structure of the knitted fabric. Analytical and FE (finite element) models have been developed [7], [10], [14] where constitutive hyperelastic models, like the Holzapfel-Gasser-Ogden model, are used. These models require fitting biaxial tensile test data, which increases the computational expense and complexity of the models.

Fabric-based pneumatic actuators use air pressure as input to control the bending motion [11]. The air pressure is usually controlled by electro-pneumatic systems, like proportional valves. To determine how much pressure needs to be input into the actuator, different control strategies for soft robotic systems

Manuscript received 14 November 2022; accepted 12 March 2023. Date of publication 5 April 2023; date of current version 14 April 2023. This letter was recommended for publication by Associate Editor S. Song and Editor Y.-L. Park upon evaluation of the reviewers' comments. This work was supported in part by the MIT School of Engineering SMA2 Brown Award, in part by the MIT Mechanical Engineering Department, and in part by the National Institutes of Health (NIH) National Institute of Biomedical Imaging and Bioengineering (NIBIB) under Grant R21-EB028414-01A1. *(Corresponding author: Ellen T. Roche.)*

Diego Quevedo-Moreno is with the Department of Mechanical Engineering, Massachusetts Institute of Technology, Cambridge, MA 02142 USA (e-mail: dquevedo@mit.edu).

Ellen T. Roche is with the Department of Mechanical Engineering, Massachusetts Institute of Technology, Cambridge, MA 02142 USA, and also with the Institute for Medical Engineering and Science, Massachusetts Institute of Technology, Cambridge, MA 02142 USA (e-mail: etr@mit.edu).

This letter has supplementary downloadable material available at https://doi.org/10.1109/LRA.2023.3264734, provided by the authors.

Digital Object Identifier 10.1109/LRA.2023.3264734

have been developed [15]. These strategies can be divided into 3 categories: model-based, model-free and hybrid-controllers. The model-based approach uses analytical models to derive the controller [16], [17], while the model-free relies on machine learning techniques or empirical methods [18], [19], [20], and the hybrid controllers combine both approaches. In this work, we propose the use of fabric shells, cut with repeating patterns and then laminated onto thermoplastic polyurethane (TPU) to form pneumatic bending actuators. This strategy avoids the use of knitted fabrics and simplifies manufacturing, modeling, and control of this class of actuators compared to other bending actuators. We characterize the blocked force of the actuator, where the maximum blocked force is 37.72+/−1.56 N, demonstrating its ability to exceed or match the analog knitted fabric-based bending actuators previously published [6], [7], [9], [10], and validating that it is suitable for applications that require high forces. We present a computational FE model that: predicts the behavior of the fabric shell design, helps to develop an intuition on how the geometrical parameters of the actuator affect its performance, and enables rapid customization of a deterministic design for future desired applications. Finally, we implement a feedback curvature control system using an empirical model-free approach to control the fabric-shelled bending actuator and achieve a precise control on its curvature. This case study is an example that showcases the benefits of this class of actuators, and provides a framework to rapidly design, manufacture, model and control tailored actuators with high force capabilities.

The remainder of this letter is organized as follows: Section II summarizes the materials and methods used to design, manufacture, characterize, model, and control the actuators proposed in this work. Section III discusses the computational and experimental results, as well as the design of the feedback control system. Finally, the conclusion and possible future work is discussed in section IV.

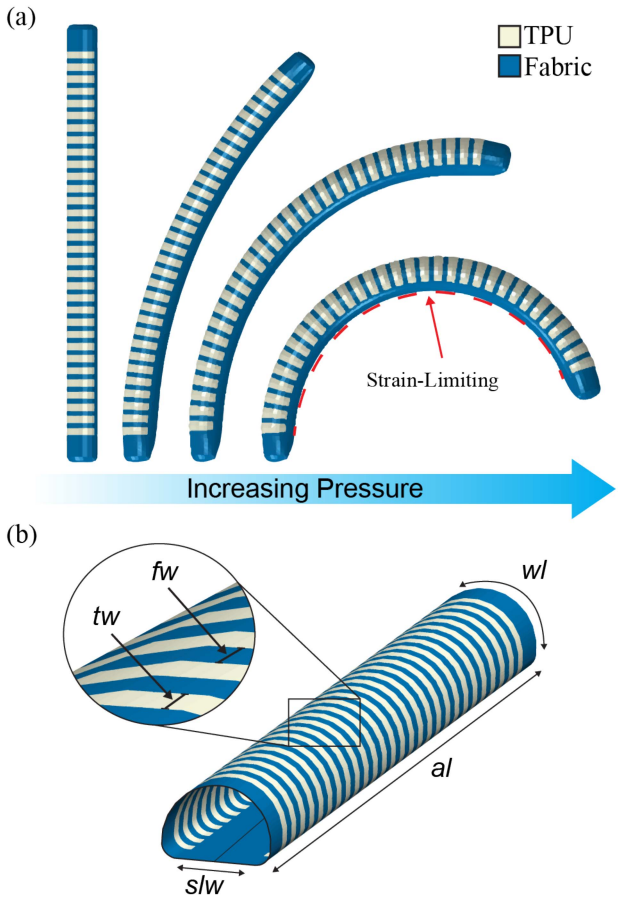

Fig. 1. Fabric-shelled bending actuator. (a) Actuator profile under different pressurization levels. (b) Fabric-shelled design. The geometrical design parameters are highlighted: actuator length (*al*), the strain-limiting layer width (*slw*), the window length (*wl*), TPU window width (*tw*) and fabric reinforcement width (*fw*).

II. Materials and Methods

A. Fabric-Shelled Soft Actuator Design

Bending soft actuators are typically comprised of two components - an extensible layer that expands upon pressurization; and an inextensible or strain-limiting layer, that restricts the expansion on one side of a given segment. The combination of these components generates bending around the neutral axis when pressurization occurs. The fabric shell design presented in this work is composed of a thermoplastic polyurethane (TPU) and an inextensible nylon woven fabric (Fig. 1(a)). Upon increasing pressurization, the TPU stretches, while the fabric acts as the strain-limiting component, constraining linear expansion and generating bending motion (Fig. 1(a)).

The fabric-shelled actuator design presented in this work (Fig. 1(b)) has various geometrical parameters that need to be defined to manufacture the shell and influence the performance of the actuator. The actuator can be fully defined by the actuator length (*al*), the strain-limiting layer width (*slw*), the window length (*wl*), the TPU window width (*tw*) and fabric reinforcement width (*fw*). The sum of the *slw* and *wl* gives the total perimeter of the semicircular cross-section of the actuator. Thus, the cross-section semicircular actuator's diameter without pressurization is defined by:

$$Actuator Diameter = (slw + wl)/\pi. \quad (1)$$

B. Fabric-Shelled Soft Actuator Fabrication

The entire manufacturing process is illustrated in Fig. 2. First, a 0.3 mm TPU-coated nylon woven fabric (6607, Rockywoods Fabric, Loveland, CO) and a 0.3 mm TPU film (78001250 M, Plastic Film Corporation of America, Lemon, IL) are cut into the desired shape using a laser cutter (VLS3.50, Universal Laser Systems, Scottsdale, AZ). Then, the resulting pieces are aligned and laminated together by using a heat-press machine (FS-DG 15 × 15 BB, FancierStudio, Hayward, CA). The lamination is possible due to the TPU coating of the nylon fabric.

A laser cut fabric strip (*slw* * *al*) is aligned with the top of the mold, the laminated piece is wrapped into the fabric strip and a 3D printed mold (Objet30 Prime 3D printer, Stratasys, Ltd., Prairie, MN) with the shape of the cavity of the actuator. Then the actuator shell is created by heat sealing at the top of the mold using a heat-press machine (Fig. 2), the fabric strip is used to

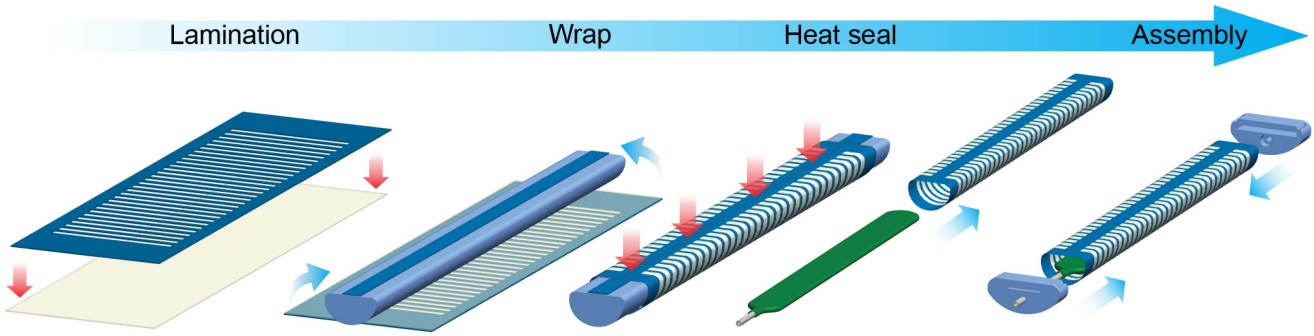

Fig. 2. Manufacturing process for fabricating fabric-shelled actuators.

TABLE I
SUMMARY OF EXPERIMENTAL AND SIMULATED RESULTS FOR THE DIFFERENT ACTUATOR DESIGNS

Parameter		Max curvature			
tw (mm)	slw (mm)	FEM (deg)	Exp (deg)	STD (deg)	Error (deg)
3	5	119.5	110.2	1.9	9.3
3	10	130.2	125.7	4.0	4.5
3	20	62.4	60.3	3.6	2.1
9	10	84.6	79.9	1.7	4.7
15	10	55.7	56.7	2.9	-1.0

join both longitudinal edges of the main laminated piece. After the shell is created, the mold is removed. A pre-fabricated thermoplastic elastomer (TPE) bladder (Stretchlon 200, FibreGlast Developments Corp., Brookville, OH) is inserted into the shell. The main purpose of the bladder is to hold air and eliminate any source of leakage, but it is oversized so that the stresses are transferred to the fabric shell and not to the internal bladder [11]. Finally, the shell is closed with 3D-printed caps. For the purpose of this study, five different actuator designs were fabricated with the following fixed parameters: Actuator Diameter = 40 mm, fw = 2 mm, and al = 180 mm, the rest of the design parameters are described in Table I.

C. Fabric-Shelled Soft Actuator Model

Predicting the nonintuitive behavior of the soft actuator is crucial to optimize and tune the actuator design according to the desired application. Although many computational models have been developed to study and predict the behavior of soft actuators [7], [10], [14], [21], none capture the characteristics of the design presented in this work. For this reason, a computational finite element (FE) model was developed to predict how the different geometrical parameters affect actuator performance.

The simulations were run using ABAQUS/Explicit (Simulia, Dassault Systemes). Surface operations were used to model the shell geometry in computer-aided design software (SolidWorks, Dassault Systemes, SE). All design parameters previously mentioned were defined.

One of the many advantages of the actuator design presented in this work is that only uniaxial testing is required to appropriately model the mechanical behavior of the materials, using constitutive models. In contrast with other FE models [7], [10], [14] that require biaxial testing to model anisotropy and use more complex constitutive models, like the Holzapfel-Gasser-Ogden model [22] or the generalized Fung model [23], which are more computationally expensive.

To model the hyperelastic material behavior of the TPU, a second order polynomial strain energy potential model was fitted into the uniaxial tensile test data experimentally obtained according to ASTM D882 guidelines using a universal testing machine (Instron 5566, 2 kN load cell, Norwood, USA). The TPU-coated nylon fabric was modeled as linear elastic with Young's modulus of 498 MPa and a Poisson's ratio of 0.35 as previously described in the literature [7]. The shell geometry was meshed using explicit linear 3-node triangular shell elements. In all simulations, the actuator was fixed at one side, and, as an input, fluid cavity pressure was applied, linearly until reaching 0.35 MPa in 2.5 seconds.

D. Control Platform

All experiments were conducted using a digital pressure regulator (ITV1031-21N2BL4, SMC Pneumatics), a microcontroller (Arduino Nano, Arduino, Somerville, MA) and a digital to analog convertor (DAC), (MCP4725, Adafruit, New York, NY) to control the pressurization of the actuator. The desired pressure is set in the microcontroller, converted into an analog signal, using the DAC module, and sent to the pressure regulator, which adjusts its internal valve to obtain the desired pressure.

E. Fabric-Shelled Actuator Blocked Force

The actuator was mounted in a universal testing machine (Instron 5566, 2 kN load cell, Norwood, MA) as shown in Fig. 3(a). Static force measurements were obtained by giving a step input pressurization with magnitudes ranging from 0.035 to 0.35 MPa with steps of 0.035 MPa. The actuator was cycled 5 times for each pressure and the peak force was recorded, this experiment was conducted three times with different fabricated actuators with the same design parameters (tw = 3 mm, fw = 2 mm, slw = 10 mm, wl = 30 mm and al = 180 mm).

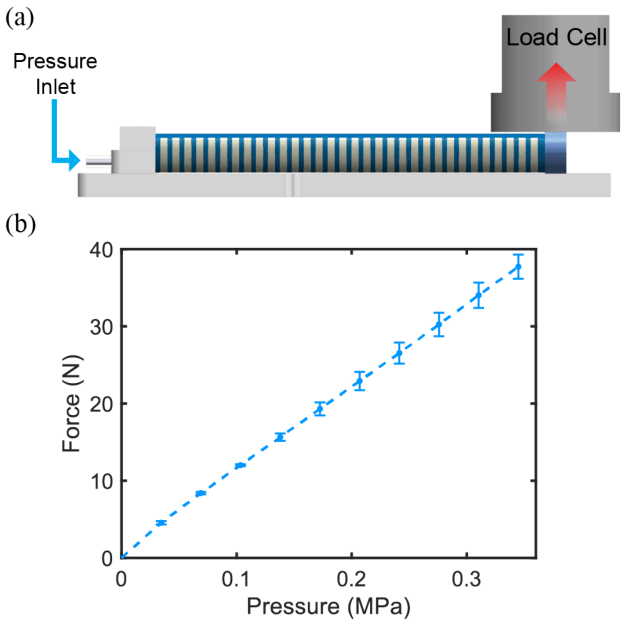

Fig. 3. Fabric-shelled Actuator Blocked Force Characterization. (a) Experimental set-up. (b) Actuator blocked force results with various pressure inputs. Error bars mean +/− standard deviation.

F. Curvature Measurements

To measure the curvature of the actuator under pressurization, one end-side of the actuator was fixed into a rigid fixture and linearly pressurized until reaching 0.35 MPa in 2.5 seconds. Red optical trackers were placed along the length of the actuator and the pressurization cycle was recorded with a camera (D3400, Nikon Corp., Tokyo, JP). Postprocessing of the video was done with a customized MATLAB script (Mathworks, Natick, MA). The position of the red markers on each frame was calculated and a circle was fitted onto the markers using direct least-squares fitting [24]. Knowing both the length of the actuator (al) and the radius of the fitted circle (r), the curvature (κ) and bending angle (θ) was calculated as using equations (2) and (3) [25]:

$$\kappa = 1/r, \tag{2}$$

$$\theta = \kappa * al. \tag{3}$$

G. Fabric-Shelled Actuator Repeatability

To evaluate the repeatability and variation of the design and manufacturing process, five samples of five different designs were fabricated. The curvature under pressurization was measured running the experiment described at the previous section (II-F). One-way ANOVA and Tukey's Honestly Significant Difference (HSD) were used to evaluate significance between different designs.

H. Feedback Control

To demonstrate the feasibility of the actuators presented in this work, a feedback control loop was implemented. An off-the-shelf resistive flexible sensor [20] (FSL095103ST, Spectra Symbol Corp., Salt Lake City, UT) was inserted into the actuator to measure the curvature in real-time and feed this signal into our control loop. Calibration of the sensor was done by reading the voltage under different pressurization levels. The curvature was calculated using the method previously described. The sensor has a linear correlation between the change in voltage and the curvature of the actuator.

The strategy implemented in this model-free approach feedback curvature controller was achieved by setting a requested curvature (K_r) and measuring the actual curvature (K_m) with the resistive flexible sensor. Then, the curvature error is calculated and compensated with a proportional-integral (PI) controller using equations (4) and (5) respectively. The proportional (k_p) and integral (k_i) gains of the controller were determined empirically. The control loop was set to run at 100 Hz.

$$e(t) = K_r - K_m \tag{4}$$

$$u(t) = k_p e(t) + k_i \int_0^t e(t)dt \tag{5}$$

Where *u(t)* is the commanded voltage (from 0 to 5 volts) to the pressure regulator. The pressure regulator reads the voltage and linearly sets the pressure, where 0 volts means 0 MPa and 5 volts means 0.48 MPa. An anti-windup method was used to limit the maximum pressure to 0.35 MPa, namely limit the commanded voltage to 3.57 volts. This type of controller guarantees zero steady-state error. The derivative term, typically used on PID controllers, is removed to reduce noise amplification of the resistive flexible sensor in the feedback control loop [20].

To evaluate the performance of the implemented control loop, a sinusoidal tracking experiment was performed. This experiment shows the ability of the actuator and of the control loop to track a curvature profile varying over time. The profile of variation is in the form of a sinusoid with a frequency of 0.2 Hz.

III. Results and Discussion

A. Fabric-Shelled Soft Actuator Design and Manufacture

The design of the soft actuator presented in this work is versatile. Geometrical parameters can be changed easily and quickly to tune the performance of the actuator, which is desirable when rapid prototyping of actuators for a specific application is required.

Compared to previous published work, this design enables the manufacture of fabric soft actuators with a laser cutter and a heat-press. Conversely, the fabrication of analogous actuators [7], [12] requires an impulse sealer, sewing machine or CNC machine with longer manufacturing processes and more expertise.

B. Fabric-Shelled Actuator Blocked Force

(Fig. 3(b)) shows the static output force of the actuator for various input pressures. The relationship between the input pressure and the output force is linear, which agrees with other soft robotic actuators [6], [7], [10]. The average maximum output force of the fabric-shelled actuator is 37.72 N with a standard deviation of 1.56 N, which exceeds the performance of fabric bending actuators previously published in the literature [6], [10],

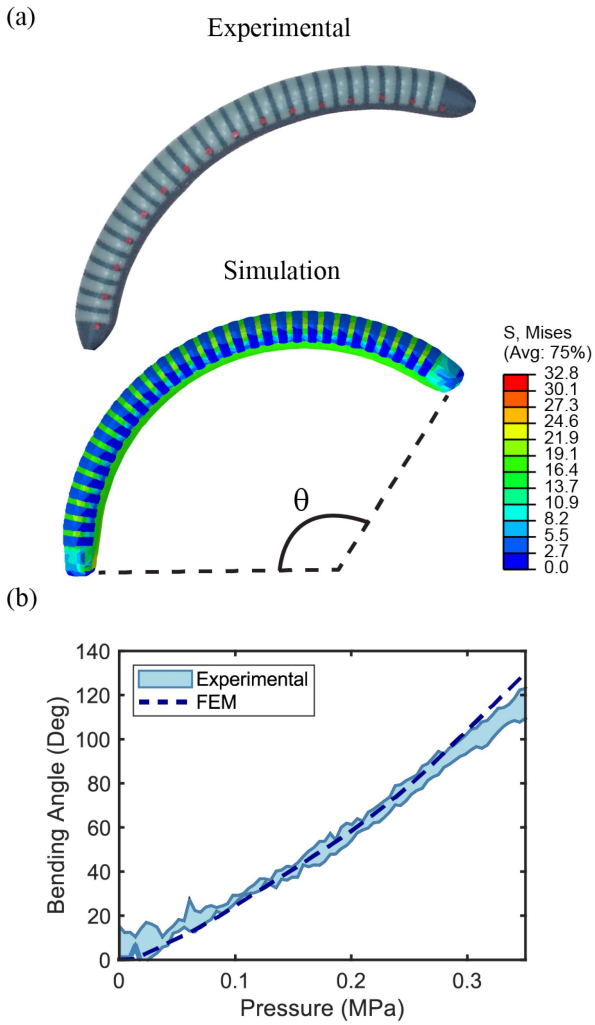

Fig. 4. Finite Element Model Validation. (a) Experimental and computational actuator's final shape at a pressurization of 0.35 MPa. (b) Fabric-shelled actuator's bending angle vs input pressure. The dashed line is the FEM results and the shaded region is the standard deviation of one actuator for three actuation cycles.

where the highest output force is 30.03 N [10]. These results motivate the utility of the fabric-shelled actuator described in this work for applications that require higher forces and low actuation volumes like locomotion assistance, grasping assistance, or haptics [3].

C. Fabric-Shelled Actuator Model

The bending angle of the actuator determined in the FE simulations closely matched with experimental results with a root-mean-square error (RMSE) of 4.97 degrees (Fig. 4). This result indicates the reliability of our FE model to predict the behavior of the shelled actuators developed in this work. The computational model developed in this work allows studying the effect of the geometrical dimensions of the fabric shells on actuator performance, such as curvature and volume, under different levels of pressurization. Even though many designs for fabric bending actuators have been developed [6], [7], [10], [14], [26], none of these studies provide insights into the sensitivity of the performance to dimensional parameters.

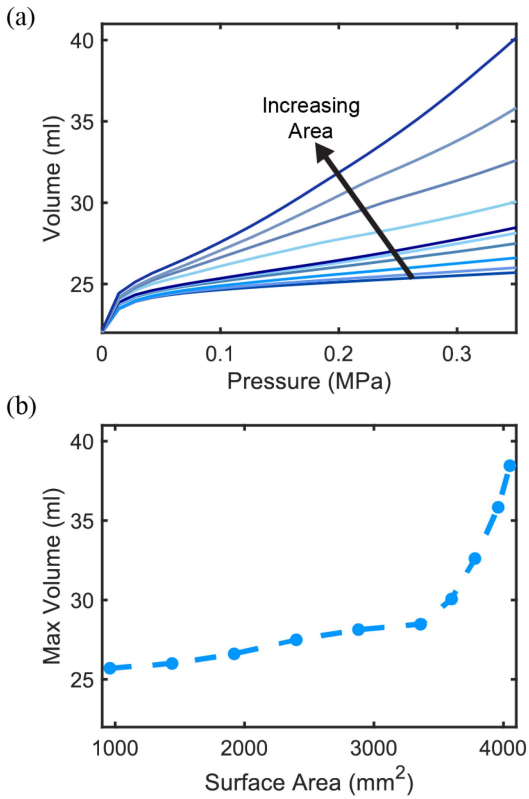

Fig. 5. Effect of TPU surface area on the actuator's volume. (a) Volume vs input pressure of different actuator designs, as the surface area of the TPU increases the curve profile goes up. (b) The maximum volume of the actuator for different actuator designs at a pressurization level of 0.35 MPa.

To inform how the dimensional parameters of the design affect the actuator's performance, namely the actuator's maximum volume and maximum curvature, two parametric studies were conducted using this FE model. First, the width of the strain-limiting layer (*slw*) was varied from 1 mm to 30 mm, then the width of the TPU window (*tw*) was varied from 1 mm to 15 mm. For the first parametric study, the following parameters were used: $tw = 3$ mm, $fw = 2$ mm, $wl = 30$ mm and $al = 180$ mm. For the second parametric study, the same dimensions were used, but the *slw* was fixed at 10 mm.

Effect of dimensional parameters on changing volume during pressurization: Understanding how the internal volume varies with different combinations of geometrical dimensions is necessary to tune the actuator design for the desired application. In the design presented in this work, the TPU window surface area (*wl* * *tw*) on the actuator plays an important role in the change of volume when pressurization occurs, as shown in Fig. 5. The total surface area of TPU on the actuator is defined by:

$$TPUarea = wl * tw * n. \tag{6}$$

Where n is the number of TPU windows on the shell design, which is defined by

$$n = (al - fw)/(tw + fw). \tag{7}$$

By increasing the *slw*, effectively decreasing *wl* (as described in (1)), the surface area of TPU is decreased. On the other hand, by increasing *tw*, the surface area of TPU is increased. Fig. 5 shows the effect of increasing the TPU area on the actuator's volume upon pressurization. At the beginning of the pressurization cycle, from 0 to approximately 0.015 MPa, the volume of the actuator increases rapidly due to the unfolding of the longitudinal edges to generate a cylindrical-like shape. Then the volume increases at a slower rate due to the stretching of the TPU window. The relationship between the TPU surface area and the actuator's volume pressurized at 0.35 MPa is presented in Fig. 5(b). The nonlinear relationship can be explained by the hyperelastic mechanical properties of the TPU. Overall, increasing the size of the TPU window width (*tw*) or decreasing the size of the *slw* increases the surface area of the TPU in the actuators, thereby, when pressurized, the more TPU stretches, the more volume the actuator is going to hold.

Effect of varying the strain-limiting layer width (slw): Fig. 6 demonstrates how the actuator's curvature is affected by increasing the width of the strain-limiting layer (*slw*), shown here at an input pressure of 0.35 MPa. When *slw* is increased from 1 mm to 10 mm the maximum curvature of the pressurized actuator increases, from 88.65 to 130.185 degrees, according to the simulated results. Experimental results show a similar effect, where changing the *slw* from 5 to 10 mm increases the maximum curvature from a mean value of 110.2 to 125.7 degrees (Fig. 6(b)). However, increasing *slw* from 10 mm to 30 mm decreases the curvature, from 130.2 to 7.8 degrees on the FE model, and experimentally from a mean value of 125.7 to 60.3 degrees when *slw* changes from 10 to 20 mm. Statistical significance of changing the *slw* parameter is shown in (Fig. 6(c)).

Effect of varying the TPU window width (tw): in Fig. 7, the effect of increasing *tw* is shown and a similar effect to varying *slw* is presented. The computational results demonstrate that the maximum curvature at pressurization increases from 74.6 to 130.2 degrees when *tw* is increased from 1 to 3 mm. However, when *tw* increases from 3 to 15 mm, the maximum curvature decreases from 130.2 to 55.7 degrees and from 125.7 to 56.7 degrees, in the simulations and experimentally, respectively. Statistical significance of changing the *tw* parameter is shown in Fig. 7(c).

Overall, the trends shown in Figs. 6 and 7 can be explained by two factors: the stretching of the TPU beyond the neutral axis of the actuator, and the stress distribution on the TPU window given the *tw* and the *wl* dimensions. When pressurized, the actuator can be considered as a cylinder, with a diameter of 40 mm, as described in (1). This cylindrical geometry has a neutral axis at its center, where the bending occurs. At *slw* of 1, 5, 10 and 15 mm, stretching of the TPU window occurs below the neutral axis, generating bending resistance [27]. Conversely, the ratio between the *wl* and the *tw* plays an important role in the stress distribution, and thus the stretch of the TPU window. This can be better understood via the mechanics of thin-walled pressure vessels [28]. When *wl* and *tw* are similar, the TPU window can be approximate as a hemisphere and all the stress

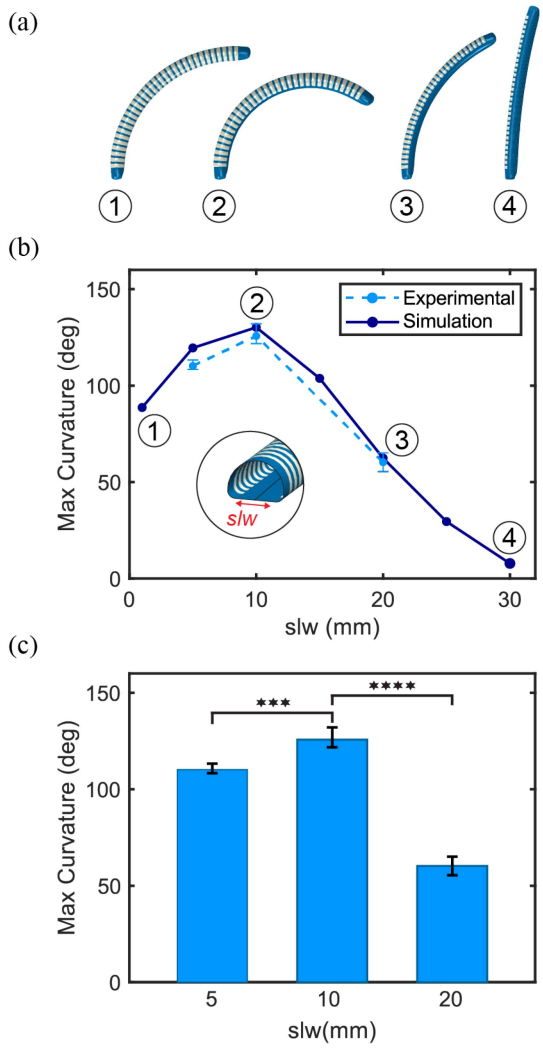

Fig. 6. Effect of varying the strain-limiting layer width (*slw*) on the curvature. (a) Actuator simulated profile of different designs pressurized at 0.35 MPa. (b) Actuator's maximum curvature of each design at 0.35 MPa. Dashed line indicates the experimental results and solid line the simulated results. (c) Experimental maximum curvature on three different designs varying *slw* (5 mm, 10 mm and 20 mm). Error bars mean +/− standard deviation of maximum curvature on five actuators for b and c. *** denotes $p < 0.0001$ and **** denotes $p < 0.00001$.

is distributed equally when pressurized. When *wl* is much larger than *tw* ($>>10$), the TPU window can be approximated as a half cylindrical pressure vessel with non-uniform stress distribution, generating more strain in the longitudinal direction and leading to bend the actuator.

A summary of the maximum curvature of the 5 different designs is presented in Table I. The mean standard deviation of the maximum curvature at 0.35 MPa for the five fabricated design is 2.8 degrees, where the highest and lowest values are 4.0 and 1.7 degrees, respectively. This demonstrated the ability of the manufacturing process to fabricate reproducible and repeatable fabric-shelled pneumatic actuators. In addition, the average error of the mean experimental maximum curvature and the FE model is 4.32 degrees, where the highest value is

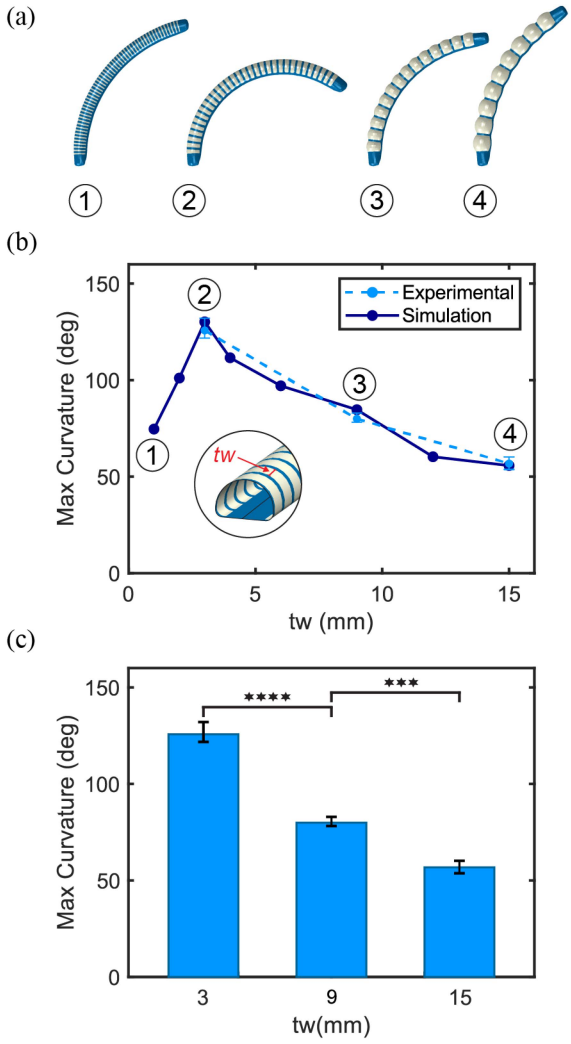

Fig. 7. Effect of varying the TPU window width (*tw*) on the curvature. (a) Actuator simulated profile of different designs pressurized at 0.35 MPa. (b) Maximum curvature of each design at 0.35 MPa. Dashed line indicates the experimental results and solid line the simulated results. (c) Experimental maximum curvature on three different designs varying *tw* (3 mm, 9 mm and 15 mm). Error bars mean +/− standard deviation of maximum curvature on five actuators for b and c. *** denotes $p < 0.0001$ and **** denotes $p < 0.00001$.

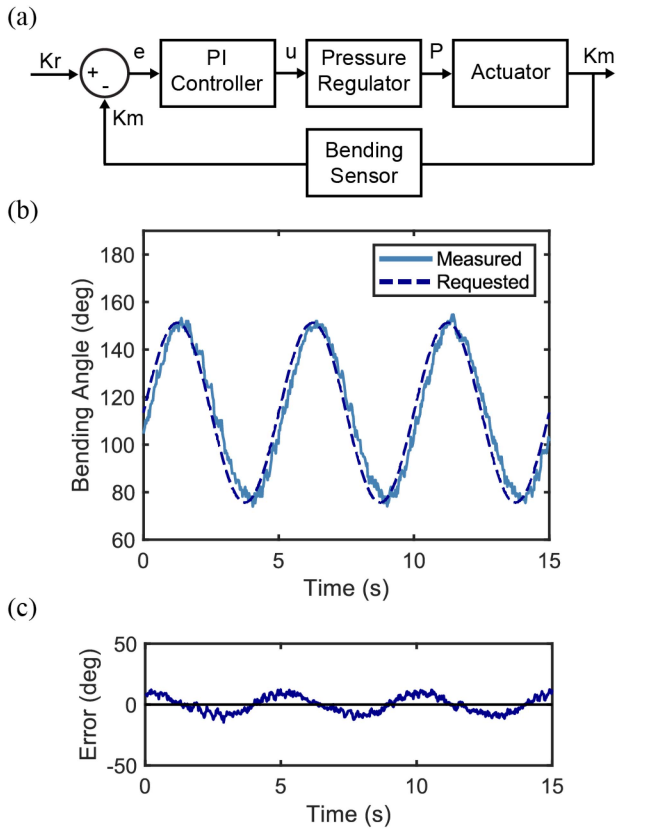

Fig. 8. Feedback Curvature Control. (a) Block diagram of the curvature control loop implemented. (b) Curvature tracking results over time. (c) Curvature error of the tracking over time.

9.0 degrees and lowest is 1.0 degrees. These results not only show the capability of the FE model to accurately predict the performance of different actuator designs but the versatility of the design to be customize for the desired bending motion.

D. Feedback Curvature Control

Using the piece-wise constant curvature model (PCC) previously described [29], the end-point position of the actuator can be precisely controlled by curvature control. In Fig. 8, the ability to control the tip position of the fabric-shelled actuator is demonstrated. Using the feedback curvature control developed in this work, the actuator can follow a curvature profile varying over time with a high correlation ($R^2 = 0.96$) and with a RMSE of 6.72 degrees, which is comparable to the error in previous published feedback controllers [22]. This error can be reduced by optimizing gains in the PI controller [20] or by implementing alternative model-based or model-free control approaches [15].

IV. Conclusion and Future Work

In this letter, a new soft actuator design, model and control was presented. The design relies on fabric shells laminated with TPU to generate soft pneumatic bending actuators. Using rapid prototyping techniques, the soft actuator is fabricated and characterized. Moreover, a FE model is developed and validated with experimental results. This model is used to predict the performance of the actuator based on variations in dimensional parameters of the shell design, showcasing the tunability and versatility of the design. These results help to inform customization for target applications like soft robotic hand exoskeletons [10], medical assist devices [30], [31], and haptic technology [3]. Finally, a method for precise position control of the actuator tip is presented by implementing a feedback control loop.

In this work, a model-free approach was used to implement a feedback curvature control. To leverage the developed FE model, future work will include the generation of a framework to compute the FE model in real time by the controller, as a model-based control approach [32]. In addition, analytical

models can be developed to account for the nonlinear behavior of the hyperelastic materials; these models will incorporate the dynamic response of the actuators to build better-informed control systems. Further, future work will include more configurations of the shell design to generate more complex motions.

REFERENCES

[1] S. Kim, C. Laschi, and B. Trimmer, "Soft robotics: A bioinspired evolution in robotics," *Trends Biotechnol.*, vol. 31, pp. 287–294, 2013.

[2] G. Agarwal, N. Besuchet, B. Audergon, and J. Paik, "Stretchable materials for robust soft actuators towards assistive wearable devices," *Sci. Rep.*, vol. 6, no. 1, pp. 1–8, 2016.

[3] V. Sanchez, C. J. Walsh, and R. J. Wood, "Textile technology for soft robotic and autonomous garments," *Adv. Funct. Mater.*, vol. 31, no. 6 2021, Art. no. 2008278.

[4] D. Rus and M. T. Tolley, "Design, fabrication and control of soft robots," *Nature*, vol. 521, pp. 467–475, 2015.

[5] C. T. O'Neill, C. M. McCann, C. J. Hohimer, K. Bertoldi, and C. J. Walsh, "Unfolding textile-based pneumatic actuators for wearable applications," *Soft Robot.*, vol. 9, pp. 163–172, 2022.

[6] C. Suulker, S. Skach, and K. Althoefer, "Soft robotic fabric actuator with elastic bands for high force and bending performance in hand exoskeletons," *IEEE Robot. Automat. Lett.*, vol. 7, no. 4, pp. 10621–10627, Oct. 2022.

[7] P. H. Nguyen and W. Zhang, "Design and computational modeling of fabric soft pneumatic actuators for wearable assistive devices," *Sci. Rep.*, vol. 10, no. 1, 2020, Art. no. 9638.

[8] C. M. Thalman, Q. P. Lam, P. H. Nguyen, S. Sridar, and P. Polygerinos, "A novel soft elbow exosuit to supplement bicep lifting capacity," in *Proc. IEEE/RSJ Int. Conf. Intell. Robots Syst.*2018, vol. 10, pp. 6965–6971.

[9] H. K. Yap et al., "A fully fabric-based bidirectional soft robotic glove for assistance and rehabilitation of hand impaired patients," *IEEE Robot. Automat. Lett.*, vol. 2, pp. 1383–1390, Jul. 2017.

[10] L. Ge et al., "Design, modeling, and evaluation of fabric-based pneumatic actuators for soft wearable assistive gloves," *Soft Robot.*, vol. 7, pp. 583–596, 2020.

[11] L. Cappello et al., "Exploiting textile mechanical anisotropy for fabric-based pneumatic actuators," *Soft Robot.*, vol. 5, pp. 662–674, 2018.

[12] P. H. Nguyen, F. Lopez-Arellano, W. Zhang, and P. Polygerinos, "Design, characterization, and mechanical programming of fabric-reinforced textile actuators for a soft robotic hand," in *Proc. IEEE Int. Conf. Intell. Robots Syst.*, 2019, pp. 8312–8317.

[13] P. H. Nguyen, Z. Qiao, S. Seidel, S. Amatya, I. I. Mohd, and W. Zhang, "Towards an untethered knit fabric soft continuum robotic module with embedded fabric sensing," in *Proc. IEEE 3rd Int. Conf. Soft Robot.*, 2020, pp. 615–620.

[14] F. Connolly, D. A. Wagner, C. J. Walsh, and K. Bertoldi, "Sew-free anisotropic textile composites for rapid design and manufacturing of soft wearable robots," *Extreme Mechanics. Lett.*, vol. 27, pp. 52–58, 2019.

[15] T. G. Thuruthel, Y. Ansari, E. Falotico, and C. Laschi, "Control strategies for soft robotic manipulators: A survey," *Soft Robot.*, vol. 5, pp. 149–163, 2018.

[16] P. Polygerinos et al., "Modeling of soft fiber-reinforced bending actuators," *IEEE Trans. Robot.*, vol. 31, no. 3, pp. 778–789, Jun. 2015.

[17] C. D. Santina, R. K. Katzschmann, A. Bicchi, and D. Rus, "Model-based dynamic feedback control of a planar soft robot: Trajectory tracking and interaction with the environment," *Int. J. Robot. Res.*, vol. 39, pp. 490–513, 2020.

[18] T. G. Thuruthel, B. Shih, C. Laschi, and M. T. Tolley, "Soft robot perception using embedded soft sensors and recurrent neural networks," *Sci. Robot*, vol. 4, 2019, Art. no. 1488. [Online]. Available: https://www.science.org

[19] C. D. Santina, R. L. Truby, and D. Rus, "Data-driven disturbance observers for estimating external forces on soft robots," *IEEE Robot. Automat. Lett.*, vol. 5, no. 4, pp. 5717–5724, Oct. 2020.

[20] G. Gerboni, A. Diodato, G. Ciuti, M. Cianchetti, and A. Menciassi, "Feedback control of soft robot actuators via commercial flex bend sensors," *IEEE/ASME Trans. Mechatron.*, vol. 22, no. 4, pp. 1881–1888, Aug. 2017.

[21] M. S. Xavier, A. J. Fleming, and Y. K. Yong, "Finite element modeling of soft fluidic actuators: Overview and recent developments," *Adv. Intell. Syst.*, vol. 3, 2021, Art. no. 2000187.

[22] G. A. Holzapfel and R. W. Ogden, "Constitutive modelling of passive myocardium: A structurally based framework for material characterization," *Philos. Trans. Roy. Soc. A: Math., Phys. Eng. Sci.*, vol. 367, pp. 3445–3475, 2009.

[23] Y. C. Fung, K. Fronek, and P. Patitucci, "Pseudoelasticity of arteries and the choice of its mathematical expression," *Amer. J. Physiol. - Heart Circulatory Physiol.*, vol. 237, no. 6, pp. H620–H631, 1979.

[24] V. Pratt, "Direct least-squares fitting of algebraic surfaces," *Comput. Graph.*, vol. 21, pp. 145–152, 1987.

[25] R. J. Webster and B. A. Jones, "Design and kinematic modeling of constant curvature continuum robots: A review," *Int. J. Robot. Res.*, vol. 29, pp. 1661–1683, 2010.

[26] G. Miron, B. Bédard, and J. S. Plante, "Sleeved bending actuators for soft grippers: A durable solution for high force-to-weight applications," *Actuators*, vol. 7, no. 3 2018, Art. no. 40.

[27] Z. Wang, P. Polygerinos, J. T. Overvelde, K. C. Galloway, K. Bertoldi, and C. J. Walsh, "Interaction forces of soft fiber reinforced bending actuators," *IEEE/ASME Trans. Mechatron.*, vol. 22, no. 2, pp. 717–727, Apr. 2017.

[28] C. T. Herakovich, "Thin-walled pressure vessels," in *A Concise Introduction to Elastic Solids*. Berlin, Germany: Springer, 2017, pp. 77–81.

[29] P. Abbasi, M. A. Nekoui, M. Zareinejad, P. Abbasi, and Z. Azhang, "Position and force control of a soft pneumatic actuator," *Soft Robot.*, vol. 7, pp. 550–563, 2020.

[30] E. T. Roche et al., "Soft robotic sleeve supports heart function," *Sci. Transl. Med.*, vol. 9, 2017, Art. no. 3925. [Online]. Available: https://www.science.org

[31] L. Hu et al., "An implantable soft robotic ventilator augments inspiration in a pig model of respiratory insufficiency," *Nature Biomed. Eng.*, vol. 7, no. 2, pp. 110–123, 2023.

[32] C. Duriez, "Control of elastic soft robots based on real-time finite element method," in *Proc. IEEE Int. Conf. Robot. Automat.*, 2013, pp. 3982–3987.